

Article

# Flood Simulations and Uncertainty Analysis for the Pearl River Basin Using the Coupled Land Surface and Hydrological Model System

Yongnan Zhu <sup>1,2</sup>, Zhaohui Lin <sup>2,3</sup>, Yong Zhao <sup>1,\*</sup>, Haihong Li <sup>1</sup>, Fan He <sup>1</sup>, Jiaqi Zhai <sup>1</sup>, Lizhen Wang <sup>1</sup> and Qingming Wang <sup>1</sup>

<sup>1</sup> State Key Laboratory of Simulation and Regulation of Water Cycle in River Basin, China Institute of Water Resources and Hydropower Research, Beijing 100038, China; zhyn@iwhr.com (Y.Z.); lihh@iwhr.com (H.L.); hefan@iwhr.com (F.H.); jiaqizhai@163.com (J.Z.); wanglz07@126.com (L.W.); wangqm@iwhr.com (Q.W.)

<sup>2</sup> International Center for Climate and Environment Sciences (ICCES), Institute of Atmospheric Physics, Chinese Academy of Sciences, Beijing 100029, China; lzh@mail.iap.ac.cn

<sup>3</sup> Collaborative Innovation Center on Forecast and Evaluation of Meteorological Disasters, Nanjing University of Information Science and Technology, Nanjing 210044, China

\* Correspondence: zhaoyong@iwhr.com; Tel.: +86-10-6878-1370

Academic Editors: Gordon Huang and Yurui Fan

Received: 23 March 2017; Accepted: 28 May 2017; Published: 1 June 2017

**Abstract:** The performances of hydrological simulations for the Pearl River Basin in China were analysed using the Coupled Land Surface and Hydrological Model System (CLHMS). Three datasets, including East Asia (EA), high-resolution gauge satellite-merged China Merged Precipitation Analysis (CMPA)-Daily, and the Asian Precipitation Highly-Resolved Observational Data Integration Towards Evaluation (APHRODITE) daily precipitation were used to drive the CLHMS model to simulate daily hydrological processes from 1998 to 2006. The results indicate that the precipitation data was the most important source of uncertainty in the hydrological simulation. The simulated streamflow driven by the CMPA-Daily agreed well with observations, with a Pearson correlation coefficient (PMC) greater than 0.70 and an index of agreement (IOA) similarity coefficient greater than 0.82 at Liuzhou, Shijiao, and Wuzhou Stations. Comparison of the Nash-Sutcliffe efficiency coefficient (NSE) shows that the peak flow simulation ability of CLHMS driven with the CMPA-Daily rainfall is relatively superior to that with the EA and APHRODITE datasets. The simulation results for the high-flow periods in 1998 and 2005 indicate that the CLHMS is promising for its future application in the flood simulation and prediction.

**Keywords:** coupled land surface-hydrology model; flood simulation; uncertainty analysis; Pearl River Basin

## 1. Introduction

Climate change caused by natural factors and human activities has been continuously aggravated in China [1,2], which has resulted in water shortages, drought and flood disasters, and other socio-economic problems. More frequent and severe extreme hydrological events have significant impacts on social development and human lives and livelihoods. Land surface hydrological models, important tools in studying the terrestrial water cycle and the related hydrological extremes, has been widely applied for watershed flood disaster forecasting and water resource protection [3,4].

Abnormal precipitation is an important factor leading to flooding and drought. As the main prognostic variable of the climate modelling and prediction, precipitation is the primary source of uncertainty in land surface and hydrological simulations [5–7]. Successful simulation of hydrological extremes under a changing climate depends strongly on spatial-temporal resolution and the accuracy

of precipitation information. China has recently developed a variety of gridded precipitation datasets with high temporal–spatial resolutions based on instrument records from ground stations and satellite products. These include the  $1^\circ \times 1^\circ$  gridded daily precipitation data established by Feng [8] with 728 stations in China;  $0.5^\circ \times 0.5^\circ$  daily precipitation data established by Chen [9] using 753 stations in China, and  $0.25^\circ \times 0.25^\circ$  daily precipitation data in China published by the National Meteorological Information Centre [10] based on 2425 stations. There are another two widely-used precipitation datasets, one is the  $0.5^\circ \times 0.5^\circ$  daily precipitation data for East Asia established by Xie [11], based on observational data from East Asian stations, and another is the  $0.25^\circ \times 0.25^\circ$  Asian Precipitation Highly-Resolved Observational Data Integration Towards Evaluation (APHRODITE) dataset developed jointly with the Japan Meteorological Agency [12].

These data have been widely applied for studying the water cycle, climate change, and related issues. However, significant uncertainties remain in the precipitation datasets from meteorological stations used for generating the final rainfall product, which will hence lead to high uncertainties in hydrological simulations. This paper takes the Pearl River—the third-longest river in China—as an example and applies the Coupled Land Surface and Hydrological Model System (CLHMS) to systematically investigate the impact of different precipitation datasets on hydrological process simulations.

## 2. Model and Method

### 2.1. Study Area

The study region in this paper is the Pearl River Basin, which contains the third-longest river in Southern China (Figure 1). The Pearl River system includes the West, East, and North Rivers and the Pearl River Delta. Measured from the headwaters of the West River, the Pearl River system has a length of more than 2300 km and a basin area of 447,000 km<sup>2</sup>, with a mild and rainy climate, which is affected by the subtropical monsoon system and tropical cyclones. The basin mean annual precipitation reaches 1525 mm, and rainfall varies throughout the year with more than 80% of annual total precipitation occurring from April to September. Owing to the large quantity of precipitation in the rainy season, with high strength and long duration, floods rapidly converge in the mountains and hills in the upper and middle reaches of the river with only few adjustable impound lakes in the middle reaches. This condition directly endangers the developed and populous cities and towns in the lower reaches. Several severe floods occurred along the Pearl River in 1998, 2000, 2005, and 2006 that directly threatened human life and property. According to incomplete statistics, flood disasters in the Pearl River that occurred between 2000 and 2013 caused more than RMB 100 billion in direct economic losses [13].

The West River is the western tributary of the Pearl River. Liuzhou and Nanning Stations are located along its tributaries, with catchment areas of 45,413 km<sup>2</sup> and 72,656 km<sup>2</sup>, respectively. Wuzhou Station, the most important control site on the main stream of the West River, has a catchment area of 327,006 km<sup>2</sup>, accounting for 94.6% of the river's catchment area. The other two main tributaries of the Pearl River are the East and North Rivers. Boluo Station is located on the lower reaches of the East River, which is the eastern tributary. The catchment area above Boluo Station is 25,325 km<sup>2</sup>, accounting for about 71.7% of the total area of the East River Basin. The catchment area above Shijiao Station, the control station for the lower reaches of the northern tributary of the Pearl River, is 38,363 km<sup>2</sup> and accounts for 82.1% of the total area of the North River Basin. The three main rivers converge in the Pearl River Delta, where the river network is staggered, and the tributaries and South China Sea simultaneously affect the water flow and water level.

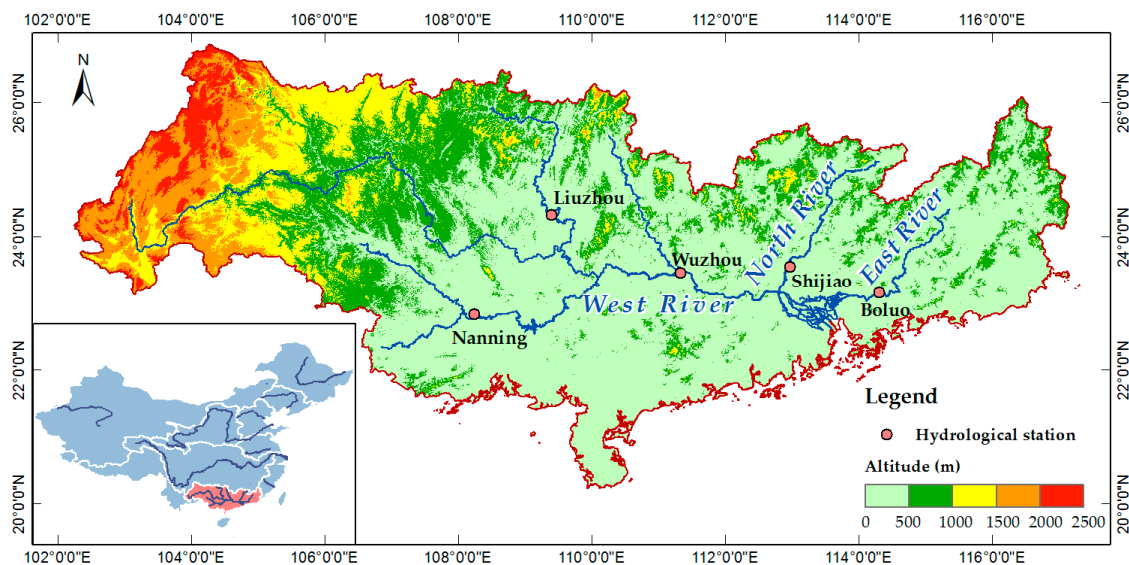


**Figure 1.** Topography of the Pearl River Basin and location of the main hydrological control stations.

## 2.2. Model Description and Simulation Design

The Coupled Land Surface and Hydrology Model System (CLHMS) is applied in this study and was briefly introduced by Yang et al. [14], developed on the basis of the Land Surface Transfer Model–Hydrologic Model System (LSX–HMS) model [15]. The CLHMS includes a large-scale LSX [16] and a fine-grid distributed HMS. The land surface model includes a two-layer vegetation module, a three-layer snow module, and a six-layer soil module. The LSX model calculates the surface energy balance and assigns the evaporation, runoff, infiltration, and soil moisture results to the HMS model. The latter includes a terrestrial hydrologic module, a groundwater hydrologic module, and a channel-groundwater interaction module. The terrestrial hydrologic module simulates overland flow and river runoff; the dynamic process of surface water flow is calculated using a two-dimensional diffusion wave in eight probable directions, and the channel flow velocity is described by the Manning equation. Groundwater is described as a single-layer aquifer and the combined water flux, including surface water, is represented by Darcy’s Law. The spatial resolution of both the land surface and hydrological models is set to  $20 \times 20$  km to avoid changing scales. The interaction between the LSX and HMS is based on predicted soil moisture and groundwater depth [15,17]. The CLHMS accurately reproduces natural hydrological processes, water balance, and seasonal and inter-annual variation in streamflow. It has been verified against historical data for the Yellow, Huai, Song-Liao, and Pearl River Basins [18–20].

Parameters in the CLHMS model include surface elevation, soil texture, vegetation type, hydro-geological parameters, and other land surface and hydrological components. The land surface soil in the CLHMS model has six layers in the upper 4.35 m; the thicknesses from the surface to the lower layer are 0.05, 0.10, 0.20, 0.40, 1.0, and 2.5 m. The soil texture character includes six layers of sand/silt/clay content from the global soil profile database generated by Webb et al. [21].

The hydrological parameters, such as slope, basin boundary, and elevation deviation are derived from the United States Geological Survey (USGS) HYDRO1k database with the ZB algorithm [22]. Other physical parameters including porosity, Manning roughness, and hydraulic conductivity are calibrated on the basis of the newest version of the Harmonized World Soil Database (HWSD) developed by the Food and Agricultural Organization (FAO) of the United Nations and International Institute for Applied System Analysis (IIASA). Launched in partnership with the Institute of Soil Science, Chinese Academy of Sciences, HWSD provides the most recent 1:1,000,000-scale subsoil and topsoil map of China [23,24].

Three high-resolution precipitation datasets—the East Asia (EA), APHRODITE, and CMPA-Daily precipitation data—were selected to investigate the impact of precipitation on the hydrological process simulation using land surface–hydrological coupled models. A brief description of the rainfall and other meteorological forcing datasets is given below.

#### (1) East Asia Daily Precipitation Data

The East Asia precipitation data was provided by the National Oceanic and Atmospheric Administration (NOAA) Climate Prediction Center (CPC) [11]. It has a spatial resolution of  $0.5^\circ \times 0.5^\circ$  and spatial extent of  $5^\circ \text{ N}–60^\circ \text{ N}$ ,  $65^\circ \text{ E}–155^\circ \text{ E}$  and covers the period 1962–2006. The data were collected by analysing the optimal difference values with the observed precipitation data from 2200 stations in East Asia, including 730 meteorological stations from the China Meteorological Administration (CMA) and 1000 hydrological observation stations from the Yellow River Conservancy Commission of the Ministry of Water Resources of the People’s Republic of China.

#### (2) APHRODITE Precipitation Data Set

The APHRODITE plan was implemented jointly by the Research Institute of Humanity and Nature (RIHN) and the Meteorological Research Institute of Japan Meteorological Agency (MRI/JMA). These agencies established a dataset describing the precipitation features of the Asian monsoon region (MA), Middle Asia (ME), Russia (RU), and Japan (JR) by integrating the observational data in the Asian regions and precipitation stations from different countries. Here, the APHRODITE dataset for monsoon Asia (APHRO-MA) was selected, which has a spatial resolution of  $0.25^\circ \times 0.25^\circ$ ; a spatial extent of  $15^\circ \text{ S}–55^\circ \text{ N}$ ,  $60^\circ \text{ E}–150^\circ \text{ E}$ ; and duration of 1951–2007. This dataset is composed primarily of station data provided by the CMA and Global Telecommunication System (GTS) data prepared by the World Meteorological Organization [12].

#### (3) High-Resolution Gauge–Satellite Merged CMPA-Daily Data

The CMPA-Daily precipitation dataset has a spatial resolution of  $0.25^\circ \times 0.25^\circ$ , a spatial extent of  $0^\circ \text{ N}–60^\circ \text{ N}$ ,  $60^\circ \text{ E}–160^\circ \text{ E}$ , and duration of 1998–2013. It uses data from 2425 national-level ground weather stations and the CPC Morphing Technique (CMORPH) data developed by the NOAA Global Precipitation Climatology Project (GPCP). The errors in CMORPH satellite precipitation data are corrected using the probability and density matching method and are generated with the optimal difference method on the basis of the climate background field [9].

To compare the uncertainty from precipitation data in land surface hydrological simulations, Three sets of contrasting numerical experiments based on CLHMS have been designed to simulate the daily water cycle process for the Pearl River during a nine-year period of 1998–2006. The three sets of experiments used the EA, APHRO-MA, and CMPA-Daily data as varying precipitation fields, whereas the other meteorology-driven data remained the same, as shown in Table 1. Four simulation experiments were designed to compare the influence of different precipitation datasets and model resolution on water cycle process simulations. In the experiments, all of the meteorological data were interpolated to the model resolution; the time steps for the hydrological and land surface models were 24 h and 15 min, respectively.

**Table 1.** Introduction to the experiment design.

No.	Test Name	Resolution	Precipitation Data Sources	Meteorological Parameters
1	EA	20 km $\times$ 20 km	Xie et al. [11]	
2	APHRO-MA	20 km $\times$ 20 km	Yatagai et al. [12]	CN05 daily temperature dataset [25];
3	CMPA-Daily (20 km)	20 km $\times$ 20 km		6-h NCEP-NCAR reanalysis data [26]
4	CMPA-Daily (10 km)	10 km $\times$ 10 km	Shen et al. [9]	

The temperature data were based on the daily temperature dataset over China (CN05) [25] from the CMA. The sub-daily data for temperature was disaggregated using statistical downscaling of

the global 3-h temperature dataset from Princeton University [27]. The near surface wind speed, humidity, air pressure, radiation flux, and other basic meteorological forcing data were obtained from the 6-h National Centres for Environmental Prediction–National Centre for Atmospheric Research (NCEP–NCAR) reanalysis data [26].

The full model was integrated with three separate processes to obtain near equilibrium groundwater tables. The first phase is the “cold start process”, in which a 50-year run was performed with the full model and observed meteorological data for 1998–2006, for the model to reach initial surface water balance. The second is the “spin-up process”, in which only the groundwater model was spun up for 5000 years using the cold start result as the forcing, in order for the model to reach equilibrium for groundwater balance. Using the model output from the “spin-up process” as initial conditions, the CLHMS was then run from 1998 to 2006 for two cycles, for 18 years in total, and the observed daily precipitation data, CN05 daily temperature data, and NCEP/NCAR six-hour reanalysis data were used as forcing data. To reduce the model bias caused by model initialization, only the model simulation results from the second cycle (year 10 to year 18) were used to analyse the water cycle from 1998 to 2006.

To correctly compare the influence of different precipitation forcings on the simulation performance of the land surface–hydrological model, the water balance index (WBI), Nash–Sutcliffe efficiency coefficient (NSE), Pearson product-moment correlation coefficient (PMC), IOA similarity coefficient, and normalized root mean square error (NRSE) were used in this study. Among these, the WBI primarily reflects the ability of the model to simulate the water quantity balance process; the NSE reflects the simulation ability for peak flow; the PMC and IOA represent the time correlation and similarity between the observed and simulated streamflow, respectively; and the NRSE is the root mean square error adjusted by the average value of the observation sequence at each site, which facilitates the comparison of different sites. For each of these five indices, values closer to one indicate higher capabilities of the model simulation. The formulae for the five indices are as follows:

$$\text{WBI} = \frac{\sum_{i=1}^N P_i}{\sum_{i=1}^N O_i}; \quad (1)$$

$$\text{NSE} = 1.0 - \frac{\sum_{i=1}^N (P_i - O_i)^2}{\sum_{i=1}^N (O_i - \bar{O})^2}; \quad (2)$$

$$\text{PMC} = \frac{\sum_{i=1}^N (P_i - \bar{P})(O_i - \bar{O})}{\left[ \sum_{i=1}^N (P_i - \bar{P})^2 \right]^{0.5} \left[ \sum_{i=1}^N (O_i - \bar{O})^2 \right]^{0.5}}; \quad (3)$$

$$\text{IOA} = 1.0 - \frac{\sum_{i=1}^N (P_i - O_i)^2}{\sum_{i=1}^N (|O_i - \bar{O}| + |P_i - \bar{P}|)^2}; \quad (4)$$

$$\text{NRSE} = 1.0 - \sqrt{\frac{1}{N} \sum_{i=1}^N \left( \frac{P_i - O_i}{\bar{O}} \right)^2} \quad (5)$$

among them,  $P_i$  and  $O_i$  are the values at the  $i$ th day simulated and observed daily streamflow, respectively;  $\bar{P}$  and  $\bar{O}$  are the average values of the simulated and observed sequences;  $N$  is the total number of samples. In this study, we selected Liuzhou, Nanning, and Wuzhou Stations on the West River, Boluo Station on the East River, and Shijiao Station on the North River as the main control sites for the Pearl River Basin. The river network in the Pearl River Delta, where the West, East, and North Rivers converge, is staggered and is influenced by the seawater intrusion, so the hydrological station in the Pearl River Delta was not selected for this study.

### 3. Analysis of Simulation Results

#### 3.1. Evaluation of Daily Simulation Performance

Figure 2 shows the simulated daily streamflow under three different precipitation forcings compared with the observed daily streamflow at the main stations in the Pearl River Basin during 1998–2006. Table 2 presents the performance of the CLHMS model based on the WBI, NSE, PMC, IOA similarity, and NRSE for Nanning, Liuzhou, Wuzhou, Shijiao, and Boluo Stations.

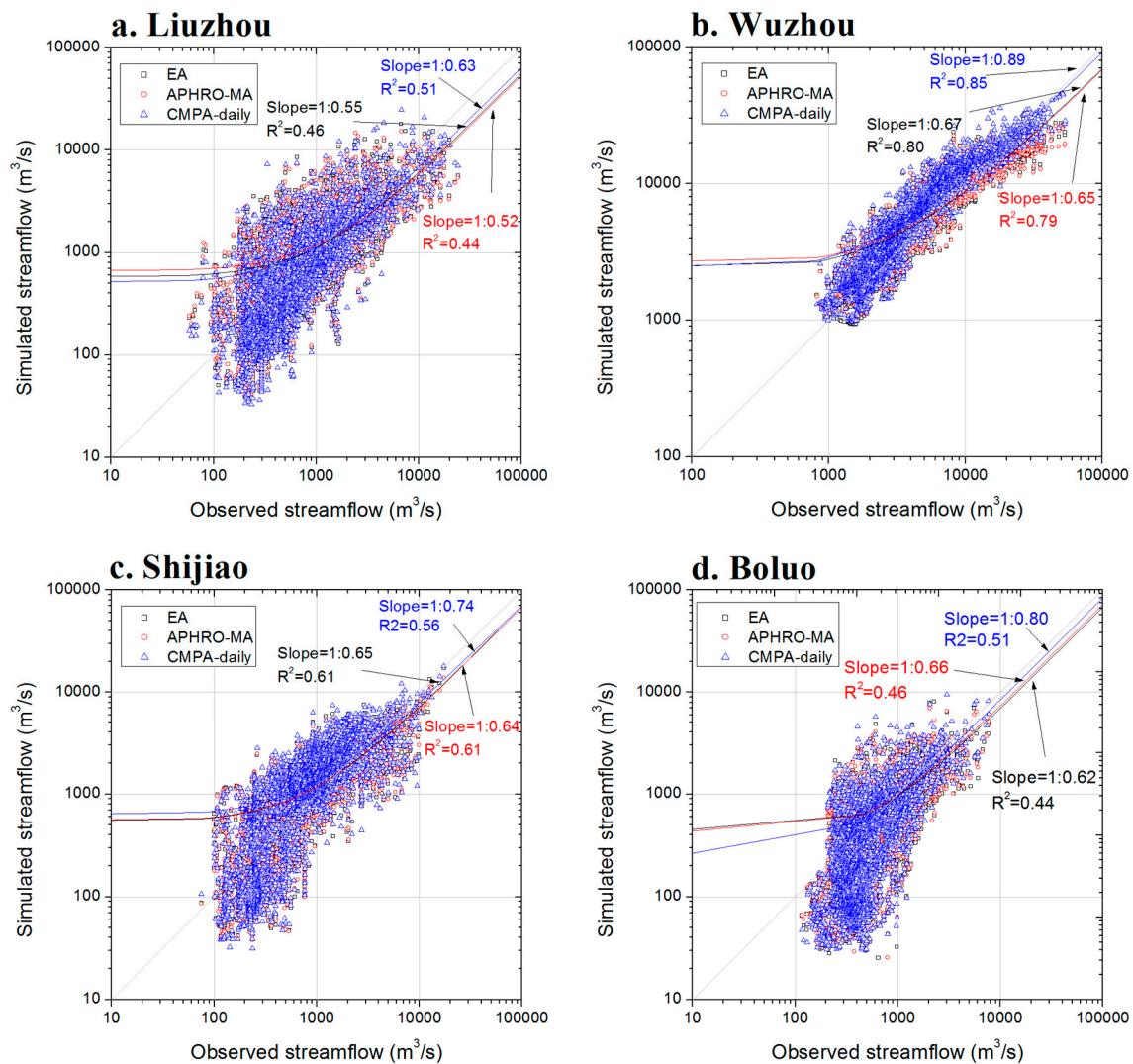


**Figure 2.** Scatterplots of a comparison between the observed streamflow and simulation from the Coupled Land Surface and Hydrological Model System (CLHMS) model for (a) Liuzhou; (b) Wuzhou; (c) Shijiao; and (d) Boluo Stations on the Pearl River from 1998 to 2006 under different precipitation forcings.

All three tests showed good simulation ability in terms of the WBI. For the simulation using the CMPA-Daily rainfall as the forcing, the PMC correlation coefficients for the Nanning, Liuzhou, and Boluo Stations were 0.63, 0.70, and 0.65, respectively, which are the highest among the three sets of simulations with different precipitation forcings. In contrast, the PMC correlation coefficients at Wuzhou and Shijiao Stations for the CMPA-Daily were 0.92 and 0.82, respectively, which shows better simulation ability in the main streams.

**Table 2.** Evaluation of the performance of the Coupled Land Surface and Hydrological Model System (CLHMS).

Hydrologic Station		Nanning	Liuzhou	Wuzhou	Shijiao	Boluo
WBI	EA	0.91	0.96	0.98	0.99	0.83
	APHRO-MA	0.93	1.01	1.00	0.99	0.86
	CMPA	0.94	1.00	1.1	1.13	0.84
NSE	EA	0.36	0.44	0.78	0.61	0.27
	APHRO-MA	0.36	0.42	0.76	0.62	0.27
	CMPA	0.38	0.47	0.81	0.67	0.25
PMC	EA	0.62	0.68	0.89	0.78	0.63
	APHRO-MA	0.61	0.66	0.89	0.79	0.64
	CMPA	0.63	0.70	0.92	0.82	0.65
IOA	EA	0.75	0.80	0.92	0.86	0.76
	APHRO-MA	0.75	0.78	0.92	0.86	0.78
	CMPA	0.75	0.82	0.95	0.90	0.77
NRSE	EA	−0.06	−0.21	0.49	0.20	0.14
	APHRO-MA	−0.06	−0.23	0.47	0.21	0.14
	CMPA	−0.06	−0.17	0.53	0.20	0.10

The NSE efficiency coefficient shows that the peak flow simulation ability of the CMPA-Daily test is obviously superior to that of the EA and APHRO-MA datasets. However, its ability to simulate the peak flow in main streams and tributaries shows a clear difference. According to the CMPA-Daily precipitation forcing, the simulated peak flow was larger than the EA- and APHRO-MA-driven simulated flow for 1998, 2000, 2001, 2004, and 2005. Taking the 1998 catastrophic flood in the West River as an example, Wuzhou Station on the main stream of the West River observed the first peak on 28 June at a flow of 51,500 m<sup>3</sup>/s; the arrival time of the peak simulated in the EA precipitation forcing test was 25 June, which is three days prior to observation. The simulated peak flow was 27,933 m<sup>3</sup>/s, which is 45.7% smaller than the observation; the peak arrival time simulated in the APHRO-MA forcing test was the same as that in the EA test. The peak flow was 26,423 m<sup>3</sup>/s, which is 48.6% smaller than the observation. The arrival time of the peak simulated in the CMPA-Daily test was 21 June, which is one day ahead of the observation. The simulation peak flow was 46,136 m<sup>3</sup>/s, which is 10.4% smaller than the observation. This flood also occurred in the North River during the same year. Shijiao Station observed the peak arrival time on 26 June with a peak flow of 12,200 m<sup>3</sup>/s; the simulated peak arrival time in the EA rainfall-driven test was 25 June, which is one day ahead of the observation. The simulation peak flow was 6681 m<sup>3</sup>/s, which is 45.2% smaller than the observation; the peak arrival time simulated in APHRO-MA test was the same as that in the EA test. The peak flow was 7621 m<sup>3</sup>/s, which is 37.5% smaller than the observation. In the simulation from the CMPA-Daily test, the peak arrival time was 24 June, and the peak flow was 9393 m<sup>3</sup>/s, which is 23.0% smaller than the observation.

A comparison of the of flow simulation result similarities under different precipitation drivers with the observation flow sequence revealed that the IOA similarity indicators for the three tests at Boluo Station were near 0.76. Those for the EA and APHRO-MA tests at Nanning, Wuzhou, and Shijiao Stations were 0.75, 0.92, and 0.86, respectively. The values were 0.75, 0.95, and 0.90, respectively, for the CMPA test. Comparing the simulation results from Liuzhou Station, the similarity for the APHRO-MA test was 0.78, which was the lowest of the three tests. The IOA similarity for the CMPA test, 0.82, was the highest. The IOA indicators for all stations under different precipitation drivers were higher than 0.75, indicating that all simulation results and observations were highly similar. The CMPA simulation results were superior those of EA and APHRO-MA.

To analyse the causes for the differences in the simulated streamflow results, we compared the differences in monthly and daily precipitation distribution from the EA, APHRO-MA, and CMPA-Daily datasets. Taking the rainstorm period in June 1998 as an example, as shown in Figure 3a–c, the maximum rainfall area appeared at the northern branch of the West River. However, some differences

in spatial distribution of the three precipitation datasets were noted. Moreover, the precipitation grid data showed a divergence in the rainfall amount. The maximum monthly rainfall of EA, APHRO-MA, and CMPA-Daily datasets were 754.59, 681.22, and 967.43 mm, respectively. Figure 3d shows the variation in the regional average daily precipitation in June 1998. The daily rainfall events of EA were essentially similar to those of APHRO-MA, except for a rainstorm on 16–26 June. Compared with the other two datasets, the CMPA-Daily rainfall events showed greater differences at the beginning of the month. For 1998–2006, the CMPA-Daily average annual precipitation in the river was 1759 mm; the values from the EA and APHRO-MA data were 1498 mm and 1525 mm in the same period, respectively. The EA and APHRO-MA precipitation data values were 14.8% and 13.3% smaller than the CMPA-Daily data, respectively. The 1998–2006 summer precipitation was also clearly different, with the CMPA-Daily, EA, and APHRO-MA precipitation data showing average summer precipitation (June–August) of 9.64, 8.12, and 8.13 mm/d, respectively.

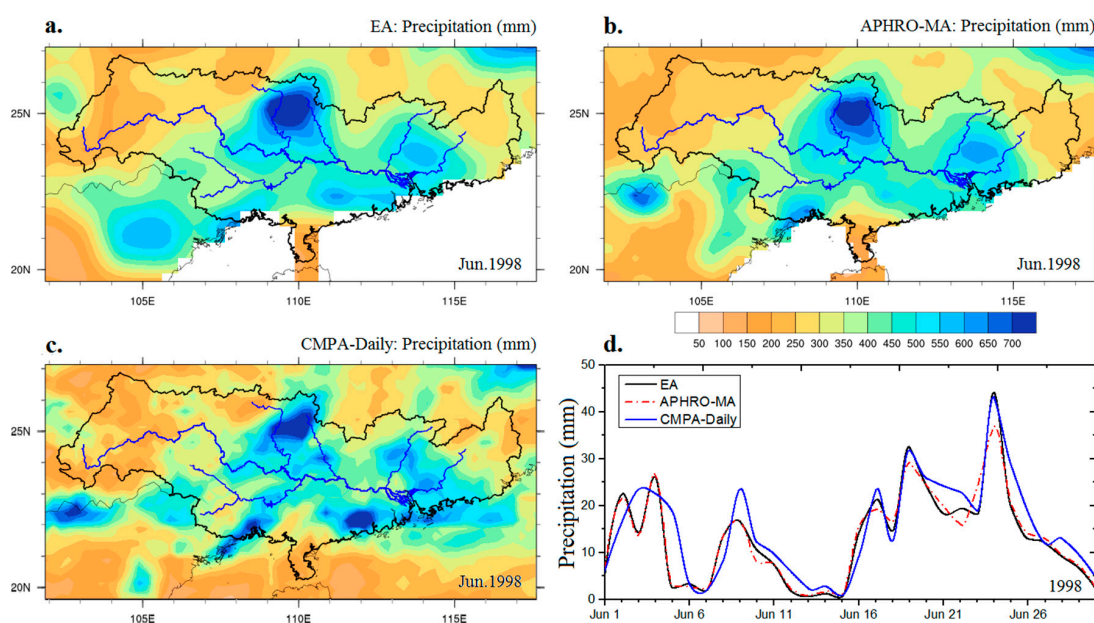


**Figure 3.** Comparison of precipitation in June 1998 for monthly rainfall distribution from (a) East Asia (EA); (b) Asian Precipitation Highly-Resolved Observational Data Integration Towards Evaluation dataset for Monsoon Asia (APHRO-MA); (c) high-resolution gauge satellite-merged China Merged Precipitation Analysis (CMPA)-Daily; and (d) the regional daily average precipitation for three precipitation forcings.

### 3.2. Evaluation of Hydrological Extreme Simulation Performance

To evaluate the CLHMS simulations of flood processes on the Pearl River, this study used the  $20 \times 20$  km and  $10 \times 10$  km grid resolution CLHMS models and the CMPA-Daily precipitation data to simulate the streamflow on the Pearl River for 11 June to 1 August 1998 and 20 May to 20 July 2005.

In June 1998, a flood with a return period of 100 years occurred on the West and North River tributaries of the Pearl River. The regional rainfall quantity exceeded 400 mm in the Liujiang and Guijiang Rivers, at the rainstorm centre. At Wuzhou Station, the maximum observation flow was  $52,900 \text{ m}^3/\text{s}$  with a recurrence interval of 100 years.

From 9 to 25 June 2005, catastrophic flooding occurred on the Pearl River owing to continuous rainstorms. At Longmen Station on the East River, the maximum precipitation reached 1442 mm. The precipitation at the rainstorm centre on the West River was 400–500 mm. At Wuzhou Station, the peak flow reached  $53,900 \text{ m}^3/\text{s}$ , which ranks as the second-highest flow since the station was established. The largest flood during the past 20 years occurred on the East River, affecting 30.32 million people and causing direct economic losses of RMB 31.45 billion [13].

Figure 4 shows the simulated and observed rainstorm processes at the main stations of the Pearl River from 11 June to 1 August 1998. Table 3 presents the simulation performance based on WBI, NSE, PMC, IOA similarity, and NRSE during the same period. The rainfall was concentrated mainly on the West and North Rivers; flooding did not occur on the East River. CLHMS simulated the flood process better at Liuzhou, Wuzhou, and Shijiao Stations, and the simulation results at Boluo Station on the East River were also consistent with the observations. During the rainstorm, three peak flooding events occurred continuously at Liuzhou Station on the West River. The third event, which occurred on 24 June, had the largest peak of the flooding process with a streamflow of 20,000 m<sup>3</sup>/s. The simulation results with 20 km resolution showed that the highest peak at Liuzhou Station occurred during the second flood event on 21 June, with a streamflow of 14,838 m<sup>3</sup>/s. In addition, the third flood event, occurring on 23 and 24 June, was lower than the previous event; this result contradicts the observations. In contrast, the simulation result from the 10 km grid resolution showed stronger similarity to the observed flood events at Liuzhou Station. The largest peak occurred on 23 June, which is one day prior to the observed event. The peak flow was 16,625 m<sup>3</sup>/s, and the simulation error was 16.9%.

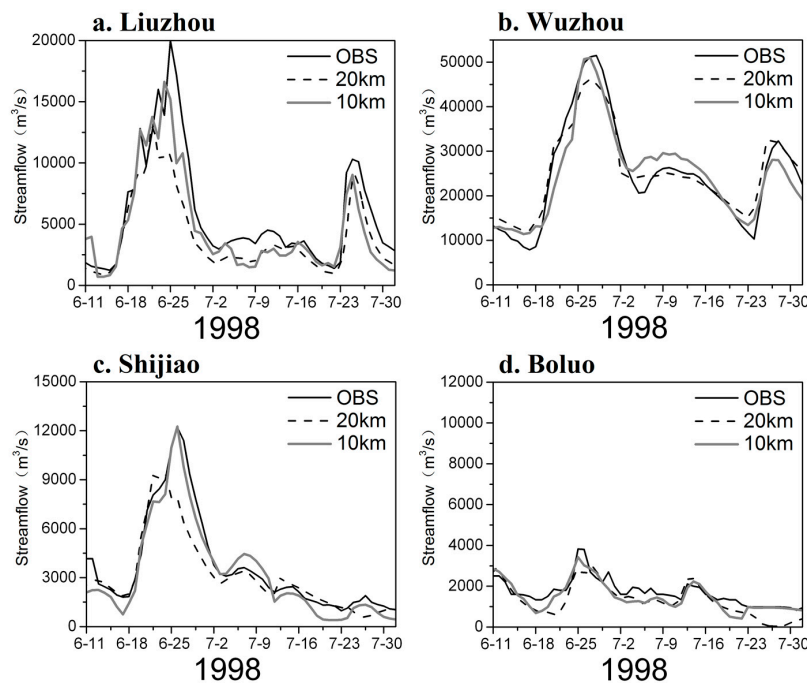


**Figure 4.** Flood simulation results for (a) Liuzhou; (b) Wuzhou; (c) Shijiao; and (d) Boluo Stations on the Pearl River in 1998.

**Table 3.** Evaluation of hydrological extremes simulation in 1998.

Hydrologic Station		Liuzhou	Wuzhou	Shijiao	Boluo
WBI	20 km	0.70	1.02	0.87	0.78
	10 km	0.82	1.00	0.90	0.87
NSE	20 km	0.62	0.93	0.80	0.22
	10 km	0.76	0.90	0.95	0.60
PMC	20 km	0.90	0.98	0.91	0.88
	10 km	0.90	0.95	0.98	0.88
IOA	20 km	0.77	0.96	0.90	0.74
	10 km	0.90	0.95	0.98	0.84
NRSE	20 km	0.52	0.96	0.62	0.67
	10 km	0.62	0.95	0.81	0.76

The measured peak flow at Wuzhou Station occurred on 28 June, when the peak flow was  $51,500 \text{ m}^3/\text{s}$ . The peak occurred on 27 June for both the 10 km and 20 km grid resolution simulations one day prior to the observed event. The simulated peak flow with 10 km resolution was  $50,988 \text{ m}^3/\text{s}$ , and the simulation error was only  $-0.4\%$ . The simulation error with 20 km resolution was  $-10.4\%$ . During the flood events in 1998, the peak flow at Shijiao Station was  $12,200 \text{ m}^3/\text{s}$ , and the peak arrival date was 26 June. The 20 km resolution simulation results showed the peak arrival date to be 24 June, which is two days prior to the observed event. The peak flow was  $9393 \text{ m}^3/\text{s}$ , which is  $23.0\%$  less than the observed flow. The peak flow was  $12,259 \text{ m}^3/\text{s}$  with 10 km resolution simulation, which is  $0.5\%$  larger than the observation, and the peak arrival time was consistent with the observation. The 20 km grid resolution simulation error in peak flow was larger. Generally, the 10 km resolution simulation of flooding of the Pearl River in 1998 is more accurate.

Figure 5 and Table 4 present the results for the flood season from 20 May to 20 July 2005. We compared the observed and simulated streamflow from the coupled land surface–hydrological model at different grid resolutions. The results showed that 10 km grid resolution provides more accurate peak flow and timing simulations and that of the simulated peak flow, which was lower than the observation when using the 20 km resolution grid. The simulations using the 20 km resolution showed a peak flow at Wuzhou Station of  $35,025 \text{ m}^3/\text{s}$ , which is  $34.3\%$  smaller than the largest peak,  $53,300 \text{ m}^3/\text{s}$ , measured on 22 June. When using the 10 km resolution grid, the simulated peak flow at Wuzhou Station was  $56,120 \text{ m}^3/\text{s}$ , which is  $5.3\%$  larger than the observed event. For both 10 km and 20 km grid resolutions, the simulated arrival date of the largest peak flow at Wuzhou Station was 20 June, which is two days prior to observation. The observed peak arrived on 24 June at Boluo Station, and the peak flow was  $7760 \text{ m}^3/\text{s}$ . When using 20 km and 10 km resolution grids, the simulated peak arrival dates were 21 June and 23 June, respectively. The simulated peak flow was  $12,430 \text{ m}^3/\text{s}$  and  $10,391 \text{ m}^3/\text{s}$ , overestimated by  $60\%$  and  $33.9\%$ , respectively. The simulation results were generally higher than the observations. According to the China water resources bulletin, 25 medium- and large-sized reservoirs were established on the Pearl River from 2001 to 2005, including five large-scale reservoirs [13]. Therefore, the regulation and control on the peak arrival time and peak flow are more important in determining the streamflow.

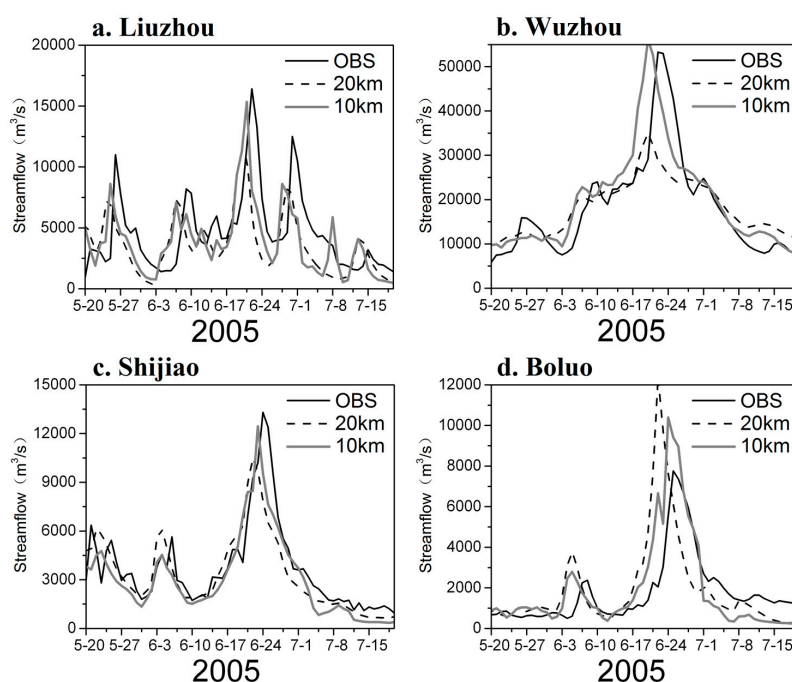


**Figure 5.** Flood simulation results at (a) Liuzhou; (b) Wuzhou; (c) Shijiao; (d) and Boluo Stations in the Pearl River in 2005.

**Table 4.** Evaluation of hydrological extreme simulation in 2005.

Hydrologic Station		Liuzhou	Wuzhou	Shijiao	Boluo
WBI	20 km	0.77	1.01	0.96	1.09
	10 km	0.66	1.09	0.88	1.04
NSE	20 km	−0.08	0.61	0.74	−0.67
	10 km	−0.46	0.66	0.61	0.40
PMC	20 km	0.43	0.83	0.86	0.46
	10 km	0.20	0.84	0.81	0.85
IOA	20 km	0.33	0.75	0.88	0.54
	10 km	0.08	0.88	0.83	0.87
NRSE	20 km	0.21	0.58	0.59	−0.31
	10 km	0.08	0.60	0.49	0.22

A comparison of the flood event simulations at the main stations of the Pearl River in 1998 and 2005 under different resolutions revealed the impact of changing water policies. Generally, the 10 km resolution grid models showed smaller simulation error in the flood arrival time and peak flow. In the model, the simulated flow of the mainstream flood in 1998 was closer to the observation. After 1998, China increased its investment in water conservancy projects, and additional facilities were used for flood regulation and control. In the Pearl River basin, 14 large reservoirs and 79 medium-scale reservoirs were built and began operation from 2000 to 2008; as a result, the total reservoir water storage increased from 21.31 billion m<sup>3</sup> in 2000 to 44.35 billion m<sup>3</sup> in 2008 [13]. The hydrological regimes of the Pearl River have also been affected by reservoirs and hydropower generation [28]. The simulated flood arrival time at the study stations occurred prior to the observed events in 2005, and the simulated peak flow at Wuzhou Station was higher than the observation. It should be noted that the model does not consider the influence of human activities on flow simulation. These overall results indicate that the skill of peak flow simulated using CLHMS still needs improvement.

#### 4. Discussion and Conclusions

Focusing on the Pearl River, this study simulated the daily streamflow time series from 1998 to 2006 with three different precipitation datasets, i.e., the EA, CMPA-Daily, and APHRODITE daily precipitation data. By comparing the simulation results with the measured streamflow, this research evaluated the model performances using different precipitation datasets as drivers in the coupled land surface–hydrological model. The results showed good model skills for simulating daily streamflow of the mainstream of the Pearl River. Driven by different precipitation data, the model simulation performances, based on indicators of water balance, efficiency coefficient, and relevant coefficient, were different. Moreover, this study showed that the average summer precipitation from the CMPA-Daily data was clearly higher than EA and APHRO-MA data for the Pearl River. The simulated daily streamflow and observed streamflow were compared using three precipitation data-driven models. The CMPA-Daily precipitation provided the best simulation of flow at the main stations of the Pearl River, which further proves that precipitation is one of the main sources of uncertainty in hydrological simulations.

The capability of CLHMS in reproducing extreme hydrological events has been verified through the simulation of two flood events in 1998 and 2005 in the Pearl River basin, and it is found that CLHMS can effectively reproduce the observed streamflow and its variation during the 1998 flood period. However, for the 2005 flood event, the peak streamflow simulated by CLHMS occurred earlier when compared with the observation. It is suggested that further efforts are needed for the improved simulation of extreme hydrological events in different years; one of these efforts could be the introduction of human activity impacts into the current coupled land surface–hydrological model system.

**Acknowledgments:** This work was jointly supported by the International Science and Technology Cooperation Program of China (grant No. 2016YFE0102400), the National Key Research and Development Program of China (grant No. 2016YFC0402702), the National Natural Science Foundation of China (grant No. 71503265), and the Special Scientific Research Fund of the Meteorological Public Welfare Profession of China (grant No. GYHY201406021). The authors would like to thank the editor and anonymous reviewers who took the time to review and provide guidance on this paper.

**Author Contributions:** Zhaohui Lin and Yong Zhao conceived and designed the experiments; Yongnan Zhu and Yong Zhao performed the model testing; Fan He, Haihong Li, Jiaqi Zhai, Lizhen Wang, and Qingming Wang contributed to the data materials; and Yongnan Zhu and Zhaohui Lin wrote the paper.

**Conflicts of Interest:** The authors declare no conflict of interest.

## References

- Zhang, J.; Wang, G.; Yang, Y.; He, R.; Liu, J. The possible impacts of Climate Change on Water Security in China. *Adv. Clim. Chang. Res.* **2008**, *4*, 290–295. (In Chinese)
- Piao, S.; Ciais, P.; Huang, Y.; Shen, Z.; Peng, S.; Li, J.; Zhou, L.; Liu, H.; Ma, Y.; Ding, Y.; et al. The impacts of climate change on water resources and agriculture in China. *Nature* **2010**, *467*, 43–51. [[CrossRef](#)] [[PubMed](#)]
- Beven, K. Dalton Medal Lecture: How far can we go in distributed hydrological modelling? *Hydrol. Earth Syst. Sci.* **2001**, *5*, 1–12. [[CrossRef](#)]
- Mauser, W.; Bach, H. PROMET—Large scale distributed hydrological modelling to study the impact of climate change on the water flows of mountain watersheds. *J. Hydrol.* **2009**, *376*, 362–377. [[CrossRef](#)]
- Krzysztofowicz, R. Bayesian theory of probabilistic forecasting via deterministic hydrologic model. *Water Resour. Res.* **1999**, *35*, 2739–2750. [[CrossRef](#)]
- Biondi, D.; De Luca, D.L. A Bayesian approach for real-time flood forecasting. *Phys. Chem. Earth* **2012**, *42–44*, 91–97. [[CrossRef](#)]
- Biondi, D.; De Luca, D.L. Performance assessment of a Bayesian Forecasting System (BFS) for real-time flood forecasting. *J. Hydrol.* **2013**, *479*, 51–63. [[CrossRef](#)]
- Feng, S.; Hu, Q.; Qian, W. Quality control of gaily meteorological data in China, 1951–2000: A new dataset. *Int. J. Climatol.* **2004**, *24*, 853–870. [[CrossRef](#)]
- Chen, D.; Ou, T.; Gong, L.; Xu, C.; Li, W.; Ho, C.; Qiang, W. Spatial interpolation of daily precipitation in China: 1951–2005. *Adv. Atmos. Sci.* **2010**, *27*, 1221–1232. [[CrossRef](#)]
- Shen, Y.; Zhao, P.; Pan, Y.; Yu, J. A high spatiotemporal gauge-satellite merged precipitation analysis over China. *J. Geophys. Res.* **2014**, *119*, 3063–3075. [[CrossRef](#)]
- Xie, P.; Yatagai, A.; Chen, M.; Hayasaka, T.; Fukushima, Y.; Liu, C.; Yang, S. A gauge-based analysis of daily precipitation over East Asia. *J. Hydrometeorol.* **2007**, *8*, 607–626. [[CrossRef](#)]
- Yatagai, A.; Arakawa, O.; Kamiguchi, K.; Kawamoto, H.; Nodzu, M.I.; Hamada, A. A 44-year daily gridded precipitation dataset for Asia based on a dense network of rain gauges. *SOLA* **2009**, *5*, 137–140. [[CrossRef](#)]
- Ministry of water resources people's republic of China. *2008 China Water Resources Bulletin*; China Water Conservancy and Hydropower Press: Beijing, China, 2009. (In Chinese)
- Yang, C.; Shao, Y.; Lin, Z.; Yu, Z.; Hao, Z.; Liu, S. Development of a two-way coupled land surface-hydrology model: Method and application. In Proceedings of the international symposium on climate change and water, Nanjing, China, 20–22 April 2011.
- Yang, C.; Lin, Z.; Yu, Z.; Hao, Z.; Liu, S. Analysis and simulation of human activity impact on streamflow in the Huaihe River Basin with a large-scale hydrologic model. *J. Hydrometeorol.* **2010**, *11*, 810–821. [[CrossRef](#)]
- Pollard, D.; Thompson, S. Use of a land-surface-transfer scheme (LSX) in a global climate model (GENESIS): The response to doubling stomatal resistance. *Glob. Planet. Chang.* **1995**, *10*, 129–161. [[CrossRef](#)]
- Yu, Z.; Pollard, D.; Cheng, L. On continental-scale hydrologic simulations with a coupled hydrologic model. *J. Hydrol.* **2006**, *331*, 110–124. [[CrossRef](#)]
- Li, M.; Lin, Z.; Yang, C.; Shao, Q. Application of a coupled land surface-hydrological model to flood simulation in the Huaihe River Basin of China. *Atmos. Ocean. Sci. Lett.* **2014**, *7*, 493–498.
- Zhu, Y.; Lin, Z.; Wang, J.; Zhao, Y.; He, F. Impacts of Climate Changes on Water Resources in Yellow River Basin, China. *Procedia Eng.* **2016**, *154*, 687–695. [[CrossRef](#)]
- Zhu, Y.; Lin, Z.; Hao, Z. Development of Large Scale Coupled Land Surface and Hydrologic Model System and Its Application in Pearl River Basin. *China Hydrol.* **2015**, *35*, 14–19. (In Chinese)

21. Webb, R.; Rosenzweig, C.; Levine, E. Specifying land surface characteristics in general circulation models: Soil profile data set and derived water-holding capacities. *Glob. Biogeochem. Cycles* **1993**, *7*, 97–108. [[CrossRef](#)]
22. Yang, C.; Yu, Z.; Lin, Z.; Hao, Z. Method Study of Constructing Digital Watershed for Large-scale Distributed Hydrological Model. *Prog. Geogr.* **2007**, *26*, 68–76. (In Chinese)
23. Shi, X.; Yu, D.; Warner, E.; Pan, X.; Petersen, G.; Gong, Z.; Weindorf, D. Soil Database of 1:1,000,000 Digital Soil Survey and Reference System of the Chinese Genetic Soil Classification System. *Soil Surv. Horiz.* **2004**, *45*, 129–136. [[CrossRef](#)]
24. Fischer, G.; Nachtergaele, F.; Prieler, S.; Velthuizen, van, H.; Verelst, L.; Wiberg, D. *Global Agro-Ecological Zones Assessment for Agriculture (GAEZ 2008)*; IIASA: Laxenburg, Austria; FAO: Rome, Italy, 2008.
25. Xu, Y.; Gao, X.; Shen, Y.; Xu, C.; Shi, Y.; Giorgi, F. A daily temperature dataset over China and its application in validating a RCM simulation. *Adv. Atmos. Sci.* **2009**, *26*, 763–772. [[CrossRef](#)]
26. Kalnay, E.; Kanamitsu, M.; Kistler, R.; Collins, W.; Deaven, D.; Gandin, L.; Iredell, M.; Saha, S.; White, G.; Woollen, J.; et al. The NCEP/NCAR 40-year reanalysis project. *Bull. Am. Meteorol. Soc.* **1996**, *77*, 437–472. [[CrossRef](#)]
27. Sheffield, J.; Goteti, G.; Wood, E. Development of a 50-year high-resolution global dataset of meteorological forcings for land surface modeling. *J. Clim.* **2006**, *19*, 3088–3111. [[CrossRef](#)]
28. Zhang, Q.; Xiao, M.; Liu, C.; Singh, V. Reservoir-induced hydrological alterations and environmental flow variation in the East River, the Pearl River basin, China. *Stoch. Environ. Res. Risk Assess.* **2014**, *28*, 2119–2131. [[CrossRef](#)]



© 2017 by the authors. Licensee MDPI, Basel, Switzerland. This article is an open access article distributed under the terms and conditions of the Creative Commons Attribution (CC BY) license (<http://creativecommons.org/licenses/by/4.0/>).